Construction of multiple anti-resonant light guidance mechanisms in a hollow core fiber structure for simultaneous measurement of multiple parameters

DEJUN LIU,[1,2] ZIYI HUANG,[1] QIANG WU,[3,4] LONG YAN,[1] KE TIAN,[5] CHANGYU SHEN,[6] GERALD FARRELL,[7] YULIYA SEMENOVA,[7] AND PENGFEI WANG[1,5,*]

[1]Key Laboratory of Optoelectronic Devices and Systems of Ministry of Education and Guangdong Province, College of Physics and Optoelectronic Engineering, Shenzhen University, Shenzhen, 518060, China
[2]Shenzhen Key Laboratory of Photonic Devices and Sensing Systems for Internet of Things, Guangdong and Hong Kong Joint Research Centre for Optical Fibre Sensors, Shenzhen University, Shenzhen, 518060, China
[3]Key Laboratory of Nondestructive Test (Ministry of Education), Nanchang Hangkong University, Nanchang 330063, China
[4]Department of Mathematics, Physics and Electrical Engineering, Northumbria University, Newcastle Upon Tyne, NE1 8ST, United Kingdom
[5]Key Lab of In-fiber Integrated Optics, Ministry Education of China, Harbin Engineering University, Harbin 150001, China
[6]Institute of Optoelectronic Technology, China Jiliang University, Hangzhou, 310018, China
[7]Photonics Research Centre, Technological University Dublin, Grangegorman Campus, Dublin, Ireland
**Corresponding author: pfwang@szu.edu.cn*

Received XX Month XXXX; revised XX Month, XXXX; accepted XX Month XXXX; posted XX Month XXXX (Doc. ID XXXXX); published XX Month XXXX

Construction of multiple light guidance mechanisms in a hollow core fiber (HCF) structure has been popular to realize simultaneous measurement of multiple parameters. In this work, a partially coating method is proposed to excite multiple anti-resonant light guidance mechanisms (ARLGMs) in an HCF structure for simultaneous measurement of multiple parameters. As an example, a double ARLGMs is demonstrated theoretically and experimentally based on a partially polyimide (PI)-coated HCF structure for simultaneous measurement of relative humidity (RH) and temperature. Dip (dip II) produced by the PI-coated HCF section shifts linearly with surrounding RH changes, with a sensitivity of circa 58.6±0.77 pm/%RH, while dip (dip I) produced by the bare HCF section (air coating layer) is insensitive to RH changes. In addition, both types of dips have linear responses to temperature variations, with similar sensitivities of ~ 17 pm/°C. Hence the proposed sensor structure can be used as an RH sensor also capable of compensating local temperature fluctuations. More importantly, simultaneous measurement of multiple parameters (such as biomarkers) is possible using the proposed method provided proper sensing materials are partially coated on the HCF surface. © 2022 Optica Publishing Group

Cross sensitivity from multiple parameters has been a serious issue for optical fiber sensors (OFSs) since it can render some sensors unusable in some cases (for example, due to failure of a material at high temperatures) or can significantly decrease the detection accuracy of a sensor. One possible solution to overcome this problem is to fabricate a high sensitivity OFS to the target parameter but with an inherent low cross-sensitivity to other possible encountered parameters [1-3]. For example, in our previous work a temperature sensor was proposed based on a small air core hollow core fiber (HCF) structure with ultra-low cross sensitivities to strain, curvature and twist [1]. Zhong et al. developed a high sensitivity temperature-independent humidity sensor based on a U-shaped plastic optical fiber evanescent-wave sensor coated with polyimide (PI) and graphene oxide layers [2]. While these approaches helped to reduce the influence of temperature, they could not fully address the issue of cross sensitivity. Another more effective and widely employed solution is a simultaneous measurement of multiple parameters by combining multiple fiber sensor structures in a common sensing system so that crosstalk influence for an OFS can be accurately accounted for and calibrated out using multiple hybrid fiber sensing structures. Highly integrated sensor head which enables multiple light guidance mechanisms is attractive for simultaneous measurement of multiple parameters due to its miniature size. Sensors based on gratings [4-5], Fabry–Perot interferometers (FPIs) [6-8] and their composite [9-10] are most investigated in the past decades.

Recently Anti-resonant guidance hollow core fiber (HCF) has been attracting considerable interest for sensing applications [11-14]. It has been demonstrated that when a bare HCF structure is coated with additional materials, the central wavelengths of the

resonant dips and their period are also dependent on the refractive index (RI) and thickness of the coating layer [15]. Hence multiple anti-resonant light guidance mechanisms (ARLGMs) could be formed by proper design the coating length and by coating different materials for different sensing purposes along the HCF so that different types of resonant dips (corresponding to different ARGMs) in transmission will be excited, and hence simultaneous measurement of multiple parameters could be achieved.

In this paper, a double ARLGMs is demonstrated as an example by partially coating Polyimide (PI) material on an HCF structure. More different ARLGMs could be excited in principle by depositing different materials along the surface of silica cladding of the proposed HCF structure (a single layer or multiple layers) and hence different sensing purposes could be achieved with such an HCF structure. Particularly in this work a humidity sensor with built-in temperature measurement is demonstrated.

The underlining light guiding principle in an HCF can be explained with an Anti-Resonant Reflecting Optical Waveguide (ARROW) model divided into two parts (A schematic diagram can be found in Fig. 1): light guiding in a bare HCF structure and light guiding in a PI-coated HCF structure. For a bare HCF structure, the silica cladding can be considered as a single layered Fabry–Perot (FP) etalon, while for a material-coated HCF structure the silica cladding and coating material can be regarded as a double layered FP etalon. Since the resonance condition is different for a single layered and a double layered FP etalons, two types of dips (dip I and dip II) with different periods can be obtained in the transmission spectrum. Their resonant wavelengths (λ_m^I, λ_m^{II}) and the corresponding free spectral ranges (FSRs) between the two adjacent resonant dips (FSR_I, FSR_{II}) can be predicted by the following equations [16]:

$$\lambda_{\mathrm{m}}^{I} = \frac{2}{m} t_1 \sqrt{n_1^2 - n_0^2} \tag{1}$$

$$\lambda_m^{II} = \frac{2}{m}\left(t_1\sqrt{n_1^2 - n_0^2} + t_2\sqrt{n_2^2 - n_0^2}\right) \tag{2}$$

$$FSR_I = \frac{\lambda_m \lambda_{m+1}}{2t_1\sqrt{n_1^2 - n_0^2}} \tag{3}$$

$$FSR_{II} = \frac{\lambda_m \lambda_{m+1}}{2\left(t_1\sqrt{n_1^2 - n_0^2} + t_2\sqrt{n_2^2 - n_0^2}\right)} \tag{4}$$

where n_0, n_1 and n_2 are the refractive indices of the air core, silica cladding and PI coating of the HCF respectively, t_1 and t_2 are the thicknesses of the silica cladding and PI coating respectively, and finally m is the resonance order (m is a nonnegative integer).

It is noted that ARLGM is excited only if the length of the HCF is longer than the critical length (L_c) which is defined as the minimum length required for light interference between I_1 and I_2. It can be derived using the ray optic method as:

$$L_c^I = \sqrt{n_0^2 + n_1^2 - n_3^2}\left(\frac{r}{\sqrt{n_3^2 - n_1^2}} + \frac{2t_1}{\sqrt{n_3^2 - n_0^2}}\right) \tag{5}$$

$$L_c^{II} = \sqrt{n_0^2 + n_1^2 - n_3^2}\left(\frac{r}{\sqrt{n_3^2 - n_1^2}} + \frac{2t_1}{\sqrt{n_3^2 - n_0^2}} + \frac{2t_2}{\sqrt{n_2^2 + n_3^2 - n_0^2 - n_1^2}}\right) \tag{6}$$

where n_3 is the RI of the SMF core, r is the radius of the hollow core of HCF. In this work, it is assumed that n_0, n_1, n_2 and n_3 are 1.0, 1.443, 1.65 and 1.449, respectively and that t_1 and t_2 are 48 μm and 12 μm. The theoretical values of L_c^I and L_c^{II} for the proposed structure are calculated to be 203.6 μm and 221.7 μm.

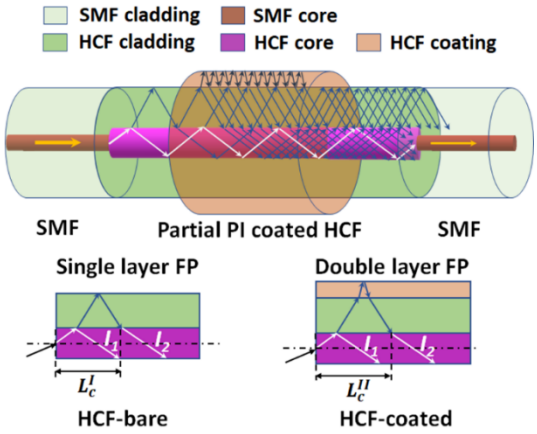

Fig. 1. A schematic diagram showing the light guiding principle in a partial PI-coated HCF structure, where arrows indicate the light transmission paths illustrated using a ray optic model. For the sake of clarity, light transmission inside the HCF structure are illustrated only for the top half of the structure.

The HCF used in experiment has an air core/cladding diameter of 30/126 μm, and a PI coating thickness of 12 μm. In particular, a section of PI-coated HCF was flame brushed on its two ends and cleaned and cleaved to a pre-set length so that a partial PI-coated HCF was fabricated. The partial PI-coated HCF was fusion spliced between two singlemode fibers (SMFs) as input and output fibers for the sensor (arc power: -75 bit, arc time: 600 ms). Sensor samples with different lengths combinations of the bare HCF (air coating layer) and PI-coated HCF sections were prepared, referred to as HCF30-A+B where the 30 indicates the air core diameter in microns, A is the length of the bare HCF section in millimeters and B is the length of the PI-coated HCF section also in millimeters. The experimental setup for temperature and RH measurement can be found in Fig. S1 in supplementary material.

The physical properties of PI are different from those of silica material and accordingly dip II and dip I behave differently with changes in the surrounding environment. To verify the prediction above with the regard the different properties of PI and silica, two samples one with no bare HCF section (HCF30-0+8) and one with a bare HCF section (HCF30-4+8) were first studied theoretically using a beam propagation method (BPM). The simulation results of the transmission spectral responses to RI changes in the PI coating are shown in Fig. 2. Strong periodic dips (marked with dashed lines) and some smaller dips are observed in the spectra for both samples. All the dips in Fig. 2(a) have similar wavelength shifts towards longer wavelengths when the RI of the PI material increases for the proposed full-length PI coated HCF structure. In contrast to this, in

Fig. 2(b) for the sample with a partial PI coating, it is observed that the strong dips (dip I type) experience only tiny changes in the central wavelengths in response to RI change, while some other smaller dips (dip II type) shift more significantly. In addition the FSRs between two adjacent strong dips around 1530 nm are measured to be 22.6 nm and 16.6 nm, which is a good match to the values from the theoretical calculation using Eqs. 3 and 4 (23.1 nm and 17.6 nm), respectively. It is thus concluded that in Fig. 2(b) the RI insensitive strong dips are a result of the effect of the bare HCF structure while other smaller dips are a result of the effect of the PI-coated HCF structure. Fig. 3 plots the wavelength shifts of selected dips with RI changes (highlighted with a rectangle in Fig. 2). In this work, a positive sensitivity is defined as that corresponding to a red wavelength shift while a negative sensitivity is related to a blue wavelength shift. Based on above definition, for dip II the bare HCF structure has an RI sensitivity of 400 nm/RIU, and a slightly reduced sensitivity of 340±15 nm/RIU for that partially PI coated HCF structure. This is reasonable since the final spectral response is a superposition of the spectra excited by a bare HCF structure and a PI-coated HCF structure and the dips sensitivities are influenced by the degree of their spectral overlap (a phase difference between two different resonant conditions) [1]. This could also explain why some of the dips of type I have a slightly larger wavelength shift. As show in Fig. 3(b), the selected dip I shows only small variations with a change in RI with a sensitivity of -21±18 nm/RIU which is over 12 times lower than that of dip II. When RH increases, the PI material well be expanded, hence the sensitivity to variations in coating thickness is also simulated as shown in Fig. S2. It shows a sensitivity around 29 nm/μm.

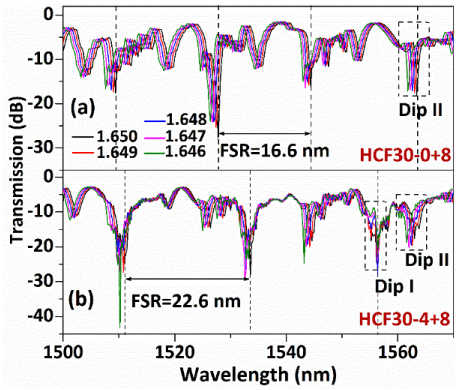

Fig. 2. (a) Simulated spectral responses to RI changes for sample (a) HCF30-0+8, and (b) HCF30-4+8.

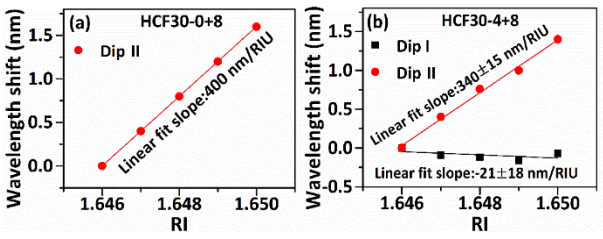

Fig. 3. (a) Simulated wavelength shifts to RI changes for sample (a) HCF30-0+8, and (b) HCF30-4+8 at selected dips.

For the partial coated HCF structure the transmission spectrum is a superposition of many different types of dips and a longer HCF section not only introduces higher loss in transmission, but also increases the strengths of many unexpected small dips, resulting in a greater difficulty in discriminating between dip I and dip II. Therefore it is critical to select an appropriate balance between the beneficial and detrimental effects of increasing the length of the bare HCF section and the PI-coated HCF section.

In experiment, investigation on length combination was first conducted as can be found in Fig. S3 in supplementary material. sample HCF30-3.9+8.4 was selected for a detailed investigation on its sensing performance for RH variations. Fig. 4 shows a few examples of the spectral responses at selected wavelengths (dip I and dip II) under various RHs when the temperature is fixed at 80 °C. As can be seen from Fig. 4, dip II moves monotonically toward longer wavelengths as the RH increases, but it is difficult to identify the central wavelength of dip I due the presence of multiple small ripples (these small ripples belong to dip II as demonstrated by its strong response to RH changes). A Gaussian fit was thus applied to the dip I data (Fig. S4 in supplementary material). The corresponding wavelength shifts versus RH for dip I and dip II are summarized in Fig. 4(c). It is found that dip II has a more linear response to RH changes with a RH sensitivity of 58.6±0.77 pm/%RH which is over 35 times higher than that of a PI-coated FBG sensor [17]. As expected, dip I is not sensitive to RH changes with a sensitivity of only 0.047 ± 0.51 pm/ %RH. The experimental results are well matched with the theoretical analysis and simulations. It is also demonstrated that the sensor's sensitivity to RH is almost independent on the operating temperature (experimental results can be found in Fig. S5 in supplementary material), which forms the basis for RH sensing with temperature calibration described below. In addition, the proposed sensor structure shows excellent measurement repeatability and good long-term stability (Fig. S6 and Table S1 in supplementary material). The measured sensor's response and recovery times are circa 6 minutes, but the actual sensor response and recovery times should be somewhat shorter since the RH recovery in the chamber is not instantaneous as can be seen from Fig. S7.

In almost all RH measurement environments, local temperature change is usually inevitable and temperature cross-sensitivity for RH sensors is a serious but common issue. Sample HCF30-3.9+8.4 was used to investigate the sensors response to temperature variations using an increase-decrease cycle while the RH was fixed at 40%. Fig. 5 (a) and (b) show examples of the spectral responses of the selected dip II and dip I wavelengths at different temperatures ranging from 20 °C to 80 °C. The corresponding wavelength shifts are plotted in Fig. 5 (c) and (d). Both dips have similar wavelength shifts towards a longer wavelength with the increase in temperature and can be linearly fitted with correlation coefficients greater than 0.996. The measured sensor sensitivity of dip II and dip I in heating and cooling processes are 17.13 pm/°C and 17.58 pm/°C, 15.93 pm/ °C and 15.63 pm/ °C, respectively. The small difference in sensitivities is most likely due to the difference in wavelength, a higher dip sensitivity is achieved at a longer wavelength [18]. It is thus concluded that for the proposed partial PI-coated HCF structure, dip II can be used for RH monitoring and the temperature influence on RH test result can be accounted by measuring the wavelength shift of dip I from the measurement result of dip II.

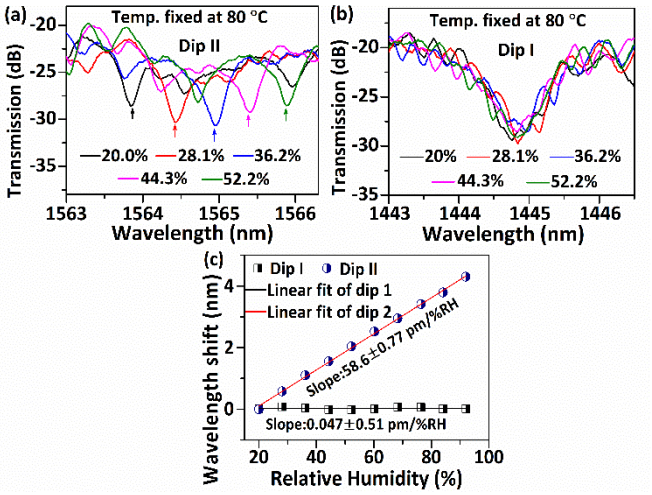

Fig. 4. Examples of measured spectral responses of selected dips for sample HCF30-3.9+8.4 at different RHs. (a) Dips II vary with RH from 20% to 52.2%, (b) Dip I varies with RH from 20% to 52.2%, and (c) Measured wavelength shifts for dips type I and type II for sample HCF30-3.9+8.4 at various RH values.

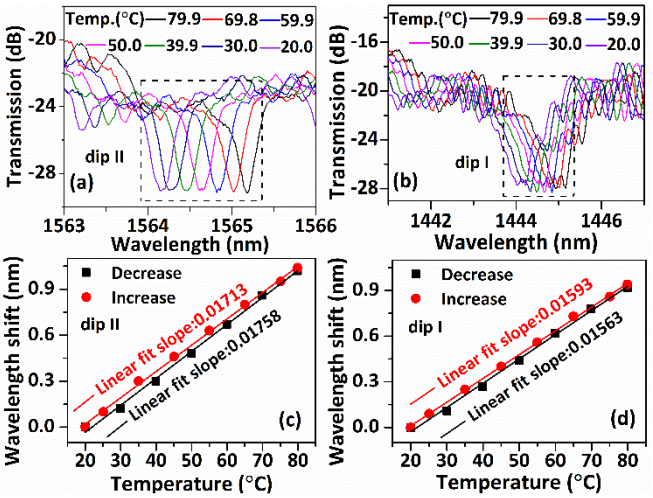

Fig. 5. Measured spectral responses of (a) dip II and (b) dip I for the sample HCF30-3.9+8.4 at different temperatures; (b) measured wavelength shifts of (c) dip II and (d) dip I at different temperatures in an increase-decrease testing cycle and their linear fits.

In conclusion, a partial coating method is proposed for construction of multiple ARLGMs in an HCF structure. In particular, a partial PI-coated HCF structure was fabricated. Both theoretical analysis and experimental results show that a double ARLGMs is present and that two independent resonant dips, namely dip I and dip II are excited by the bare HCF and PI-coated HCF sections, respectively. It is found that dip II is highly sensitive to the surrounding RH changes with a sensitivity of circa 58 pm/%RH while dip I is RH-insensitive with a sensitivity as low as 0.96 pm/%RH. Both dips have similar temperature sensitivities around 17 pm/°C. Therefore, dip II can be used for RH monitoring while dip I can be used for temperature sensing as a means to mitigate temperature cross-sensitivity. When proper sensing materials are partially coated on the HCF surface, the proposed sensor structure could be a good candidate to be used in practical applications such as simultaneous measurement of multiple types of biomarkers for medical diagnostics.

Funding. National Natural Science Foundation of China (62105217, 11874332); Guangdong Basic and Applied Basic Research Foundation (2019A1515110320); Shenzhen Fundamental Research Program (JCYJ20190808173401660, JCYJ20190808140805488, JCYJ20190808173619062); National Key Scientific Instrument and Equipment Development Projects of China (61727816).

Disclosures. The authors declare no conflicts of interest.

Data availability. Data underlying the results presented in this paper are not publicly available at this time but may be obtained from the authors upon reasonable request.

Supplemental document. See Supplement 1 for supporting content.

References

1. D. Liu, W. Li, Q. Wu, F. Ling, K. Tian, C. Shen, F. Wei, G. Farrell, Y. Semenova, and P. Wang, Opt. Express **29**, 26353 (2021).
2. N. Zhong, X. Xin, H. Liu, X. Yu, H. Chang, B. Tang, D. Zhong, M. Zhao, H. Zhang, and J. Zhao, Appl. Opt. **59**, 5708 (2020).
3. C. Zhou, Q. Zhou, B. Wang, J. Tian, and Y. Yao, Opt. Express **29**, 11854 (2021).
4. J. Hromadka, N. N. M. Hazlan, F. U. Hernandez, R. Correia, A. Norris, S. P. Morgan, and S. Korposh, Sens. Actuators B Chem. **286**, 306 (2019).
5. J. Madrigal, D. Barrera, and S. Sales, IEEE J. Sel. Top. Quantum Electron. **26**, 5600306 (2020).
6. J. Tian, Y. Z. Jiao, S. B. Ji, X. L. Dong, and Y. Yao, Opt. Commun. **412**, 121 (2018).
7. S. Pevec and D. Donlagic, Opt. Lett. **40**, 5646 (2015).
8. C. Zhou, Q. Zhou, C. He, J. Tian, Y. Sun, and Y. Yao, IEEE Sensors J. **21**, 9877 (2021).
9. Y. Liu, X. Liu, T. Zhang, and W. Zhang, Opt. Laser. Eng. **111**, 167–171 (2018).
10. Y. Liu, D. Yang, Y. Wang, T. Zhang, M. Shao, D. Yu, H. Fu, and Z. Jia, Opt. Commun. **443**, 166–171 (2019).
11. D. Liu, Q. Wu, C. Mei, J. Yuan, X. Xin, A. K. Mallik, F. Wei, W. Han, R. Kumar, C. Yu, S. Wan, X. He, B. Liu, G. Peng, Y. Semenova, and G. Farrell, J. Lightwave Technol. **36**, 1583 (2018).
12. D. Liu, R. Kumar, F. Wei, W. Han, A. K. Mallik, J. Yuan, C. Yu, Z. Kang, F. Li, Z. Liu, H. Tam, G. Farrell, and Y. Semenova, J. Lightwave Technol. **36**, 3672 (2018).
13. M. Hou, F. Zhu, Y. Wang, Y. Wang, C. Liao, S. Liu, and P. Lu, Opt. Express **24**, 27890 (2016).
14. Q. Wu, Y. Qu, J. Liu, J. Yuan, S. Wan, T. Wu, X. He, B. Liu, D. Liu, Y. Ma, Y. Semenova, P. Wang, X. Xin, and G. Farrell, IEEE Sens. J. **21**, 12734 (2021).
15. R. Gao, Y. Jiang, and Y. Zhao, Opt. Lett. **39**, 6293 (2014).
16. X. Zhang, H. Pan, H. Bai, M. Yan, J. Wang, C. Deng, and T. Wang, Opt. Lett. **43**, 2268 (2018).
17. J. Zhang, X. Shen, M. Qian, Z. Xiang, and X. Hu, Opt. Fiber Technol. **61**, 102406 (2021).
18. Y. Liu and L. Wei, Appl. Opt. **46**, 2516–2519 (2007).

Full References

1. D. Liu, W. Li, Q. Wu, F. Ling, K. Tian, C. Shen, F. Wei, G. Farrell, Y. Semenova, and P. Wang, "Strain-, curvature- and twist-independent temperature sensor based on a small air core hollow core fiber structure," Opt. Express **29**(17), 26353–26365 (2021).
2. N. Zhong, X. Xin, H. Liu, X. Yu, H. Chang, B. Tang, D. Zhong, M. Zhao, H. Zhang, and J. Zhao, "Plastic optical fiber sensor for temperature-independent high-sensitivity detection of humidity," Appl. Opt. **59**(19), 5708–5713 (2020).
3. C. Zhou, Q. Zhou, B. Wang, J. Tian, and Y. Yao, "High-sensitivity relative humidity fiber-optic sensor based on an internal–external Fabry–Perot cavity Vernier effect," Opt. Express **29**, 11854-11868 (2021)
4. J. Hromadka, N. N. M. Hazlan, F. U. Hernandez, R. Correia, A. Norris, S. P. Morgan, and S. Korposh, "Simultaneous in situ temperature and relative humidity monitoring in mechanical ventilators using an array of functionalised optical fibre long period grating sensors," Sens. Actuators B Chem. **286**, 306–314 (2019).
5. J. Madrigal, D. Barrera, and S. Sales, "Regenerated Fiber Bragg Gratings in Multicore Fiber for Multi-Parameter Sensing," IEEE J. Sel. Top. Quantum Electron. **26**(4), 5600306 (2020).
6. J. Tian, Y. Jiao, S. Ji, X. Dong, and Y. Yao, "Cascaded-cavity Fabry-Perot interferometer for simultaneous measurement of temperature and strain with cross-sensitivity compensation," Opt. Commun. **412**, 121–126 (2018).
7. S. Pevec and D. Donlagic, "Miniature all-silica fiber-optic sensor for simultaneous measurement of relative humidity and temperature," Opt. Lett. **40**(23), 5646–5649 (2015).
8. C. Zhou, Q. Zhou, C. He, J. Tian, Y. Sun, and Y. Yao, "Fiber optic sensor for simultaneous measurement of refractive index and temperature based on internal-and-external-cavity Fabry-Pérot interferometer configuration," IEEE Sensors J. **21**(8), 9877–9884 (2021).
9. Y. Liu, X. Liu, T. Zhang, and W. Zhang, "Integrated FPI-FBG composite all-fiber sensor for simultaneous measurement of liquid refractive index and temperature," Opt. Laser. Eng. **111**, 167–171 (2018).
10. Y. Liu, D. Yang, Y. Wang, T. Zhang, M. Shao, D. Yu, H. Fu, and Z. Jia, "Fabrication of dual-parameter fiber-optic sensor by cascading FBG with FPI for simultaneous measurement of temperature and gas pressure," Opt. Commun. **443**, 166–171 (2019).
11. D. Liu, Q. Wu, C. Mei, J. Yuan, X. Xin, A. K. Mallik, F. Wei, W. Han, R. Kumar, C. Yu, S. Wan, X. He, B. Liu, G. Peng, Y. Semenova, and G. Farrell, "Hollow Core Fiber Based Interferometer for High-Temperature (1000 °C) Measurement," J. Lightwave Technol. **36**(9), 1583–1590 (2018).
12. D. Liu, R. Kumar, F. Wei, W. Han, A. K. Mallik, J. Yuan, C. Yu, Z. Kang, F. Li, Z. Liu, H. Tam, G. Farrell, and Y. Semenova, "Highly Sensitive Twist Sensor Based on Partially Silver Coated Hollow Core Fiber Structure," J. Lightwave Technol. **36**(17), 3672–3677 (2018).
13. M. Hou, F. Zhu, Y. Wang, Y. Wang, C. Liao, S. Liu, and P. Lu, "Antiresonant reflecting guidance mechanism in hollow-core fiber for gas pressure sensing," Opt. Express **24**(24), 27890-27898 (2016).
14. Q. Wu, Y. Qu, J. Liu, J. Yuan, S. Wan, T. Wu, X. He, B. Liu, D. Liu, Y. Ma, Y. Semenova, P. Wang, X. Xin, and G. Farrell, "Singlemode-Multimode-Singlemode Fiber Structures for Sensing Applications–A review," IEEE Sens. J. **21**(11), 12734–12751 (2021).
15. R. Gao, Y. Jiang, and Y. Zhao, "Magnetic field sensor based on anti-resonant reflecting guidance in the magnetic gel-coated hollow core fiber," Opt. Lett. **39**(21), 6293–6296 (2014).
16. X. Zhang, H. Pan, H. Bai, M. Yan, J. Wang, C. Deng, and T. Wang, "Transition of Fabry–Perot and antiresonant mechanisms via a SMF-capillary-SMF structure," Opt. Lett. **43**(10), 2268–2271 (2018).
17. J. Zhang, X. Shen, M. Qian, Z. Xiang, and X. Hu, "An optical fiber sensor based on polyimide coated fiber Bragg grating for measurement of relative humidity," Opt. Fiber Technol. **61**, 102406 (2021).
18. Y. Liu and L. Wei, "Low-cost high-sensitivity strain and temperature sensing using graded-index multimode fibers," Appl. Opt. **46**(13), 2516–2519 (2007).